nature communications

Article

https://doi.org/10.1038/s41467-024-52010-4

Entangling gates on degenerate spin qubits dressed by a global field

Received: 16 January 2024

Accepted: 21 August 2024

Published online: 03 September 2024

Check for updates

Ingvild Hansen[1] ✉, Amanda E. Seedhouse[1,2], Santiago Serrano[1], Andreas Nickl[1], MengKe Feng[1,2], Jonathan Y. Huang[1], Tuomo Tanttu[1,2], Nard Dumoulin Stuyck[1,2], Wee Han Lim[1,2], Fay E. Hudson[1,2], Kohei M. Itoh[3], Andre Saraiva[1,2], Arne Laucht[1,2], Andrew S. Dzurak[1,2] ✉ & Chih Hwan Yang[1,2] ✉

Semiconductor spin qubits represent a promising platform for future large-scale quantum computers owing to their excellent qubit performance, as well as the ability to leverage the mature semiconductor manufacturing industry for scaling up. Individual qubit control, however, commonly relies on spectral selectivity, where individual microwave signals of distinct frequencies are used to address each qubit. As quantum processors scale up, this approach will suffer from frequency crowding, control signal interference and unfeasible bandwidth requirements. Here, we propose a strategy based on arrays of degenerate spins coherently dressed by a global control field and individually addressed by local electrodes. We demonstrate simultaneous on-resonance driving of two degenerate qubits using a global field while retaining addressability for qubits with equal Larmor frequencies. Furthermore, we implement SWAP oscillations during on-resonance driving, constituting the demonstration of driven two-qubit gates. Significantly, our findings highlight how dressing can overcome the fragility of entangling gates between superposition states and increase their noise robustness. These results constitute a paradigm shift in qubit control in order to overcome frequency crowding in large-scale quantum computing.

In the race towards building a large-scale universal quantum computer, we are faced with several potential future bottlenecks. The fragility of qubits is a commonly discussed aspect as current quantum error correction codes, essential for fault tolerant quantum computing, only allow for very small error rates[1]. The scaling prospect is also of utmost importance, since the number of required physical qubits is expected to exceed millions. Challenges include routing of necessary control signals onto the quantum processor chip[2], control signal interference, variability[3], etc. Scaling up current architectures by brute force will present many challenges and is not necessarily the best course of action.

Global control was suggested by Kane in 1998[4] and involves globally applying a single microwave field to an array of qubits. Recent advancements have demonstrated a version where the qubits are by-default on resonance[5–7]. Dressed qubits are continuously decoupled from low-frequency noise and individually addressed by local electrodes[6,8]. Furthermore, the global field can be generated off-chip[9,10], which frees up space on the chip and simplifies control signal routing. Therefore, a global control scheme based on dressed degenerate qubits tackles the fragility of qubits while offering a prospect for scalability. Additional advantages include reduced control bandwidths and control signal interference.

[1]School of Electrical Engineering and Telecommunications, The University of New South Wales, Sydney, NSW, Australia. [2]Diraq, Sydney, NSW, Australia. [3]School of Fundamental Science and Technology, Keio University, Yokohama, Japan. ✉e-mail: ingvild.hansen@ntnu.no; a.dzurak@unsw.edu.au; henry.yang@unsw.edu.au

In this work, we demonstrate two crucial components of the vision to operate dressed degenerate qubits in a global field, namely single-qubit addressability and two-qubit operation. We tune two silicon metal-oxide-semiconductor (SiMOS) quantum dot spin qubits (see Supplementary Fig. 1) such that their Larmor and Rabi frequencies are matched, and then perform single- and two-qubit universal dressed control in a global field.

Results

Degenerate spins in a global dressing field

Traditionally, qubits are addressed by their individual Larmor frequencies using spectral selectivity[11–13], as illustrated in Fig. 1a. To avoid interference between different control signals, this strategy requires a spread of Larmor frequencies in excess of the Rabi frequency. The Larmor frequency of a qubit is set by the Bohr magneton, the static magnetic field strength B_0 and the g-factor. The latter has a natural variability in Si/SiO_2 devices (~ MHz/T) due to spin-orbit coupling[3,11,14–16]. Nanomagnets resulting in a slanted field can also be used such that qubits in different locations see different magnetic field strengths[17–20]. With these aforementioned strategies one can control a handful of qubits[18,19,21–23]. However, when scaling up to millions of qubits, frequency crowding will become a problem[5,24]. Moreover, due to the distribution of Larmor frequencies, the native two-qubit gate between neighbouring spins, which is a function of the Larmor frequency difference and the exchange magnitude, varies between controlled-Z (CZ) and SWAP[25].

The aim of a global control strategy using dressed qubits is to have arrays of quasi-degenerate spins that can be driven on-resonance by a global microwave field (GHz range) and addressed individually by local electrodes (MHz range), as illustrated in Fig. 1b. As opposed to conventional electron-spin-resonance (ESR) control, as well as electric-dipole spin resonance (EDSR) control, individual addressing allows for signals in the MHz range, instead of in the GHz range. This approach circumvents the problem of frequency crowding and control signal interference when scaling up. Conveniently, the SWAP gate is the native two-qubit gate for quasi-degenerate spins due to the small Larmor frequency differences[25].

To drive multiple qubits with a global field, it is favourable for the qubits to be uniform, and it has been shown recently that the variability of SiMOS spin qubits caused by the roughness of the Si/SiO_2 interface is bounded[3]. The g-factor variability is expected to be < 0.1 % for a DC magnetic field applied along the {100} direction and the robust control protocol introduced in refs. 6,7 and employed in ref. 26 is designed to handle this bounded variability.

Here, we consider two quantum dots formed underneath plunger gates P1 and P2, with a barrier gate J1 in between and mimic the behaviour of a global control field with an ESR antenna and therefore have to carefully match the Larmor and Rabi frequencies. The qubit Larmor frequencies must all be within the linewidth of the global microwave field in order to achieve on-resonance driving and the Rabi frequencies must be similar, so that the qubits follow the same clock cycle. A sizeable Stark shift from the top gates on the Larmor frequencies is also important for addressability.

Larmor frequency matching

The g-factor variability from spin-orbit interactions can be minimised by pointing the static magnetic field along {100} instead of the default direction {110}[3,14]. The {100} magnetic field orientation can also reduce the qubit susceptibility to charge noise and potentially increase T_2^*[14,27]. Although this strategy is useful for matching the Larmor frequencies of two qubits, one can not rely on this alone when scaling up to larger numbers of qubits. Using low static magnetic field strength is also beneficial for the qubit uniformity[12], as the Larmor frequency variability is directly proportional to the g-factor times the static magnetic field ($\nu \propto gB_0$). Applying large microwave powers increases the Rabi frequency, and therefore also increases the tolerable spread of qubit Larmor frequencies.

By ramping the voltage detuning between quantum dots at a determined rate, we initialise the system in the $|\downarrow\uparrow\rangle$ spin state, facilitated by the fact that near the charge transition the spins are not yet entirely degenerate. We then study the voltage dependence of the qubit frequencies by performing slow chirped microwave pulses, which adiabatically invert the spin state if its resonance frequency is contained within the range of the chirp[28] (see more details in

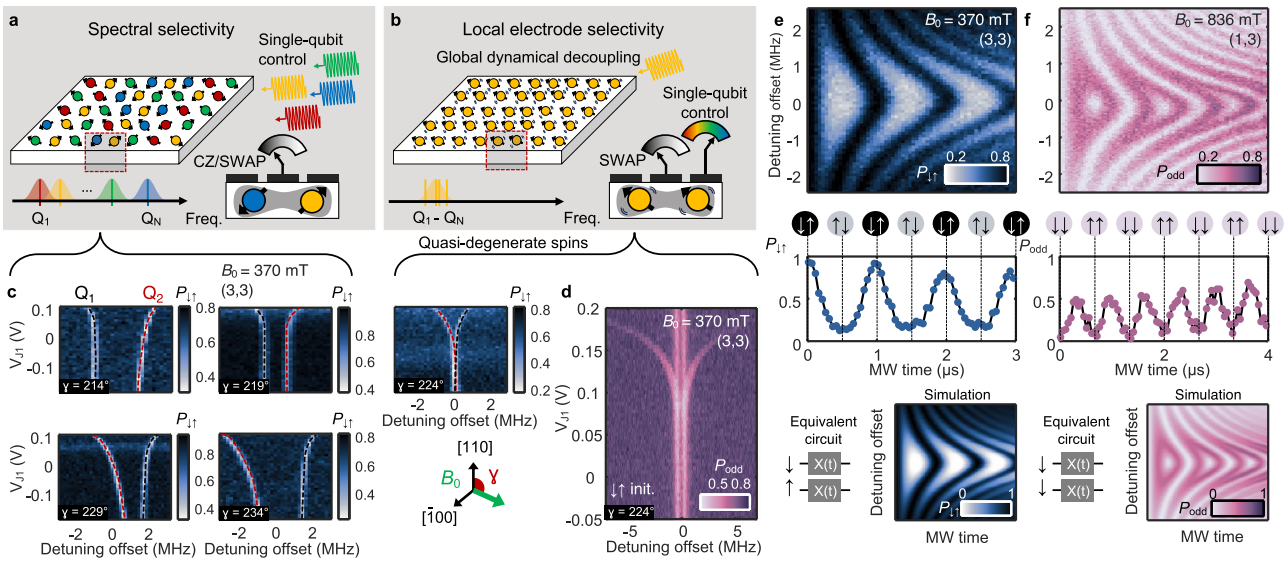

Fig. 1 | Degenerate spin qubits in a global field. Operation using (**a**) spectral selectivity of non-degenerate spins and (**b**) local electrode selectivity of degenerate spins for individual qubit control. **c** Adiabatic inversions of two spins with varying in-plane static magnetic field angle γ using $|\downarrow\uparrow\rangle$ initialisation and adiabatic singlet-triplet (ST) readout. The frequency detuning is offset for each sub-panel. **d** High-resolution adiabatic inversion with parity readout at $\gamma = 224°$ where the spin qubits are quasi-degenerate. **e**, **f** Rabi chevrons of quasi-degenerate spins simultaneously driven by a global field with adiabatic ST and parity readout, respectively. The initial states are $|\downarrow\uparrow\rangle$ and $|\downarrow\downarrow\rangle$, respectively, with Larmor frequencies 10.362 GHz and 23.221 GHz. Traces at the centre frequencies are plotted below. Circuit models and simulations are shown in the bottom of (**e**) and (**f**).

Supplementary Note 4). This is verified by measuring the probability that the final spin state is blockaded, as plotted in Fig. 1c.

Adiabatic spin inversions as a function of V_{J1} with different static magnetic field angles γ are shown. At $\gamma = 224^{\circ}$, near the $[\bar{1}00]$ orientation, the two qubits are quasi-degenerate. Note that after this angle, the order of the qubit frequencies inverts and therefore the initialisation also inverts, resulting in the reflection of the branching of the frequencies as a function of V_{J1}. In Fig. 1d, a high-resolution version of the quasi-degenerate case is shown with Larmor frequencies around 10.362 GHz, separated by < 200 kHz. This small difference in Larmor frequency is achieved by pointing the static magnetic field along $[\bar{1}00]$, which minimises the Dresselhaus spin-orbit coupling, and using a relatively low magnetic field strength of 370 mT.

The difference between spin Zeeman energies, combined with other parameters, is known to shift the outcome of the spin blockade from a singlet-triplet (ST) readout to a parity readout[29]. In the present case, the $|\downarrow\uparrow\rangle$ state is mapped into the unblockaded singlet through an adiabatic ramp in some configurations (which we refer to as adiabatic ST), while in others any odd-parity state ends up equally unblockaded (see Supplementary Note 3). Once the operational parameters are settled, a characterisation is required to distinguish between the two scenarios.

Rabi frequency matching

When the Larmor frequencies of two qubits match, as demonstrated at low V_{J1} in Fig. 1d, they can be driven simultaneously with a global field. The resulting Rabi frequency is set by the power delivered to the qubits from the microwave source, through the on-chip ESR antenna. Due to the transmission characteristics of the ESR antenna, the power delivered into the device varies as a function of microwave frequency (and therefore the Rabi frequency depends on the choice of B_0). Moreover, the Rabi frequencies of the two qubits are not necessarily equal. Besides the inhomogeneity of the oscillatory magnetic field generated by the antenna geometry, both qubits can be affected by the spurious electric component of the microwave field[30]. This electric drive is usually minimised through the choices of double-dot electrostatic potential confinement, static magnetic field strength and orientation.

The only scalable way to address this variability in Rabi frequency is to engineer the microwave field to have minimal electric component. In the particular case of two qubits, however, we can tolerate the stray electric fields by fine-tuning the magnetic field strength until the Rabi frequencies of both qubits match. We find both Larmor frequency matching and Rabi frequency (Ω_R) matching with values 10.362 GHz and 1 MHz, respectively, at 370 mT. The Larmor frequencies are different by $< 20\%$ of Ω_R and the Rabi frequencies by $< 5\%$ of Ω_R. These conditions lead to qubit rotations that are sufficiently synchronous to consider the two qubits simultaneously driven with a shared clock (and any deviations are considered coherent errors in the qubit operations).

In Fig. 1e, a Rabi chevron is shown for two qubits with matched Larmor and Rabi frequencies in the adiabatic ST readout regime with $|\downarrow\uparrow\rangle$ initialisation. Here, $X(t) = \exp(-i\Omega_R\sigma_x t)$ when the detuning offset is zero. The same is shown in Fig. 1f for the parity readout regime with $|\downarrow\downarrow\rangle$ initialisation. The adiabatic ST readout yields a periodic oscillation at the Rabi frequency but it is not a simple sinusoidal because only the $|\downarrow\uparrow\rangle$ is unblockaded, while the driving populates all states (see Supplementary Note 3 for detailed explanation). The parity readout regime gives oscillations at twice the frequency and half the amplitude when initialised in $|\downarrow\downarrow\rangle$, due to $|\downarrow\uparrow\rangle$ and $|\uparrow\downarrow\rangle$ both being unblockaded. All the following measurements are done using $|\downarrow\uparrow\rangle$ initialisation and the adiabatic ST readout regime.

By leveraging advanced microwave engineering and a dielectric resonator or a cavity as the microwave source in the future, increasing the magnitude and uniformity of the magnetic field, the matching conditions for Larmor and Rabi are not expected to present a significant challenge.

Entanglement during on-resonance driving

The fundamental interaction between spins is the spherically symmetric Heisenberg exchange coupling $H_X = J\boldsymbol{\sigma_1}\cdot\boldsymbol{\sigma_2}$. In the particular case of non-degenerate spin qubits, the Larmor frequency difference creates an effective Ising coupling $H_I = J\sigma_{z,1}\sigma_{z,2}$, which favours the implementation of CZ gates. In the case of degenerate qubits the full Heisenberg interaction naturally leads to SWAP gates instead, as originally proposed by Loss and DiVincenzo[5,25,31–34]. When qubits are driven at the same Larmor and Rabi frequency they are effectively under the same rotating frame such that the J operator commutes with the global field ([IX+XI,SWAP]=0).

A voltage pulse applied to gate J1 (see Supplementary Fig. 1) turns the exchange interaction on and off, showing SWAP oscillations over time in Fig. 2a as a function of V_{J1}. The fastest SWAP oscillation recorded here is ~100 ns, limited by the voltage range of the equipment (see Methods). Differently from the case of CZ, where a strong exchange coupling leads to deviations from the idealised Ising model, here the stronger the exchange further accentuates the Heisenberg interaction.

We repeat the same entangling pulse measurement in the case when a microwave on resonance with both qubits is applied with either a constant power or with a sinusoidal modulation, shown in Fig. 2b and c, respectively. Note that the V_{J1} pulse is centred within the microwave pulse, however, this is not a requirement. The microwave pulse duration is fixed to ensure that it effectively performs an identity gate. We find that the SWAP oscillations remain unchanged during microwave driving but lose some visibility, which we attribute to degradation of the SET charge readout caused by heating. The sinusoidal modulated driving is found to be more robust against Larmor frequency variability (see Supplementary Fig. 2).

In Fig. 2d–f, we showcase the most important result in this work, that the SWAP oscillations between superposition states[35] are significantly more preserved for driven qubit implementations than for bare qubits. Looking at the experiment in Fig. 2a–c this point is missed because the SWAP oscillations between the states $|\uparrow\downarrow\rangle$ and $|\downarrow\uparrow\rangle$ are not exposed to T_2 decoherence times the whole time. In fact, the continuous swapping of $|\downarrow\uparrow\rangle$ and $|\uparrow\downarrow\rangle$ serves as an echoing sequence doing an effective Hahn echo in the J basis, echoing out dephasing noise. However, SWAP oscillations between the more relevant $(|\uparrow\downarrow\rangle \pm |\downarrow\uparrow\rangle)/\sqrt{2}$ states reveal the true impact of decoherence on these states and the benefits of dynamical decoupling.

We repeat the measurement with initial states varying continuously from $|\downarrow\uparrow\rangle$ ($\theta = 0$) to $|\uparrow\downarrow\rangle$ ($\theta = \pi$) with a microwave pulse to rotate the qubits before a fixed V_{J1} pulse and undo the rotation at the end. Here, $X(\theta) = \exp(-i\sigma_x\theta/2)$. For initialisations around $\theta = \pi/2$, the driven SWAP oscillations remain coherent for longer than in the undriven case. This can be explained by noise decoupling[36–38] resulting from the driving field[6] (see noise simulations in Supplementary Note 5). Crucially, our results draw attention to the fragility of entangling gates between arbitrary superposition states (as opposed to eigenstates, see Supplementary Fig. 3), which are typically not studied in literature[32–34,39]. In Fig. 2g–i, the oscillations for initialisation in $|y\rangle \otimes |\bar{y}\rangle$ (dotted line at $\theta = \pi/2$ in Fig. 2d–f) are compared. Being able to perform $\mathrm{SWAP}/\sqrt{\mathrm{SWAP}}$ on arbitrary states with high fidelity is not only important in universal quantum computing for implementing two-qubit computational gates, but also in the context of coherent quantum state transfer[24].

Joint coherence metrics

In Fig. 3a and b, free-induction decay and Hahn echo measurements are performed. In the context of simultaneously driven qubits, however, these experiments must be reinterpreted. The joint

https://doi.org/10.1038/s41467-024-52010-4

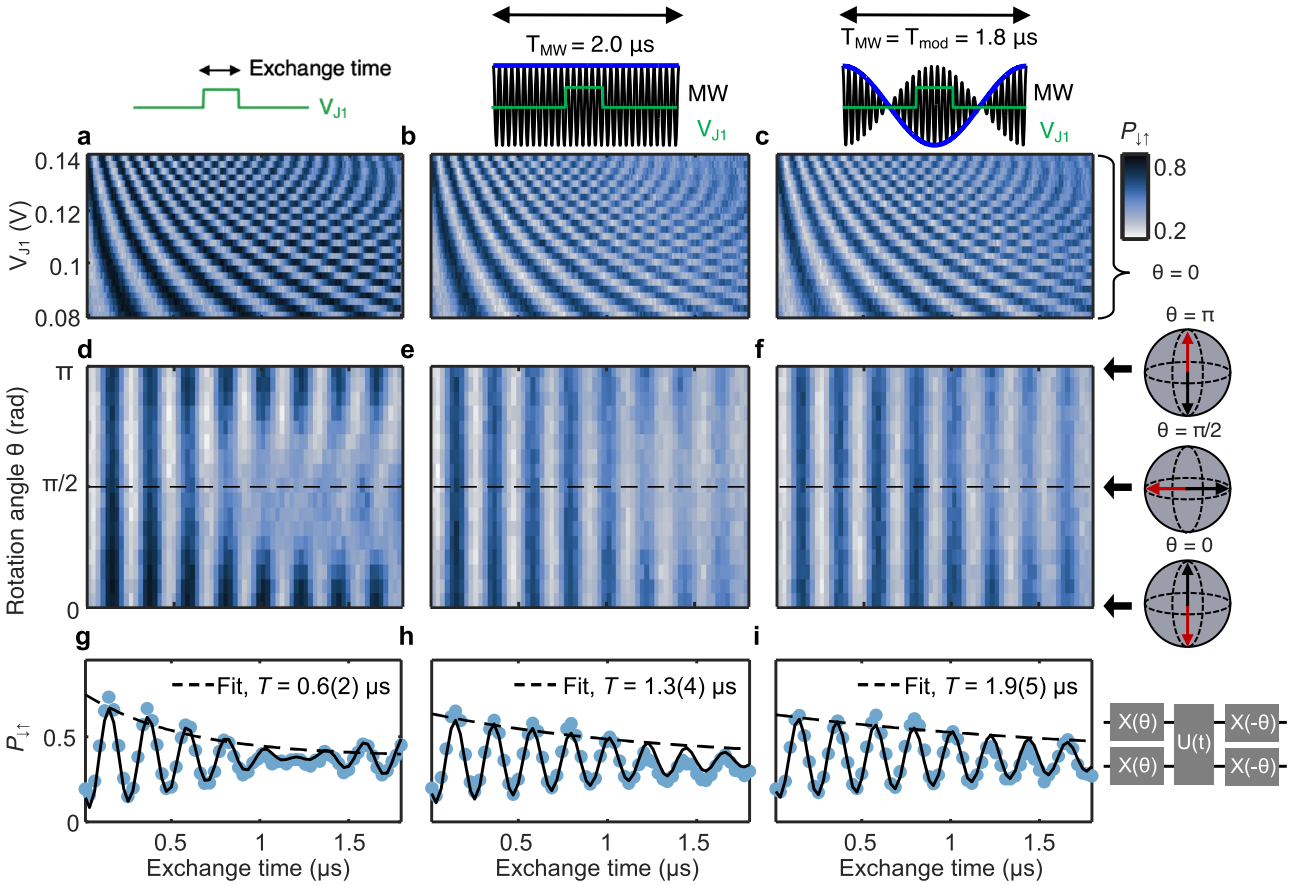

Fig. 2 | Entanglement between on-resonance driven arbitrary spin states. SWAP oscillations during (**a**) no microwave drive, **b** continuous wave microwave of duration $T_{MW} = 2.0\,\mu$s with $\Omega_R = 1$ MHz, and (**c**) sinusoidal modulated microwave of duration $T_{MW} = T_{mod} = 1.8\,\mu$s. The microwave is applied along the *x*-axis and the modulation is according to $\sqrt{2}\Omega_R \cos\left(2\pi T_{mod}^{-1} t\right)$. **d**–**f** Initialisation of arbitrary states between $|\downarrow\uparrow\rangle$ and $|\uparrow\downarrow\rangle$ where θ is the rotation angle of the projection pulses and $V_{J1} = 0.1$ V. The state of the spins after the initial projection is $X(\theta) \otimes X(\theta)|\downarrow\uparrow\rangle$. In (**g**)–(**i**), the traces at $\theta = \pi/2$ ($|y\rangle \otimes |\bar{y}\rangle$ initialisation) are plotted and fitted, the solid line fits the theorised spin dynamics (see Supplementary Note 6) and dashed line fits an exponential decay of the in-phase SWAP oscillations. All data is acquired in an interleaved manner. At zero time $P_{\downarrow\uparrow} \neq 1$ for all V_{J1}, despite $|\downarrow\uparrow\rangle$ initialisation, due to bandwidth limitations of the cables causing exchange interaction during the ramp.

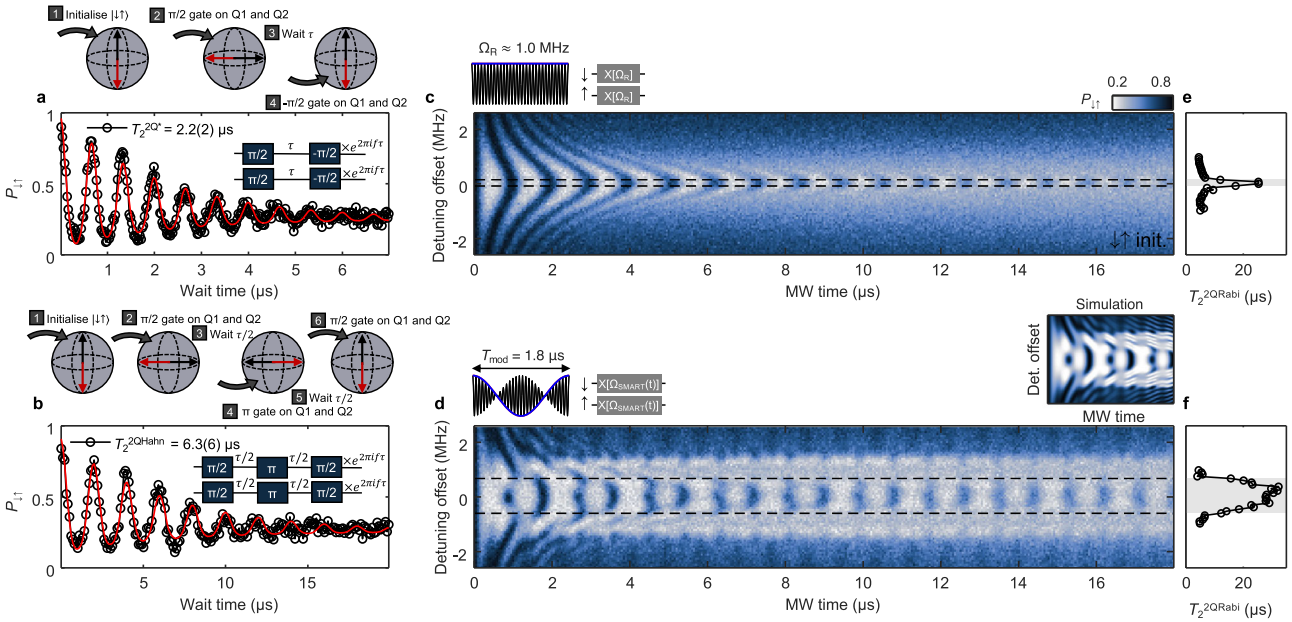

Fig. 3 | Coherence metrics of degenerate qubits. a Free-induction decay and (**b**) Hahn echo measurement applied to degenerate qubits, where oscillations of frequency *f* are introduced for fitting purposes. Chevron with (**c**) square modulation and (**d**) sinusoidal modulation acquired in an interleaved manner where the global microwave frequency is swept. Here, $\Omega_{SMART}(t) = \sqrt{2}\Omega_R \cos\left(2\pi T_{mod}^{-1} t\right)$. The extracted T_2^{2QRabi} times are plotted in (**e**) and (**f**) and the grey shaded area represents $T_2^{2QRabi} > 10\,\mu$s.

probabilities $P_{\downarrow\uparrow}$ oscillate (similar to Fig. 1e) because the recovery $\pi/2$ gate is applied at an angle increasing with wait time τ in regard to the preparation gate (these oscillations are introduced to improve the fitting accuracy). The decay of these oscillations is the joint decay rate of the two spins, which are simultaneously prepared in superposition states $|+y\rangle = 1/\sqrt{2}(|\uparrow\rangle + i|\downarrow\rangle)$ and $|-y\rangle = 1/\sqrt{2}(|\uparrow\rangle - i|\downarrow\rangle)$. This is different from regular Hahn echo and Ramsey experiments where the ancilla qubit is typically kept in a protected eigenstate and not exposed to dephasing. If the decoherence processes are completely independent, both the free-induction and Hahn echo decays are expected to be twice as fast as the conventional single-qubit measurements. We extract $T_2^{2Q^*} = 2.2(2)\,\mu s$ and $T_2^{2QHahn} = 6.3(6)\,\mu s$, where the superscript 2Q refers to the fact that both qubits are involved in the dephasing.

In Fig. 3c and d, we show the driven two-qubit oscillations over time as a function of the microwave frequency in the case of optimally matched Larmor and Rabi frequencies. The constant power case (Fig. 3c) is the same experiment as shown before in Fig. 1e, but now with sufficiently long times to observe the decay of the driven qubits. The horizontal dashed lines indicate the range of detunings that yield $T_2^{2QRabi} > 10\,\mu s$. This arbitrary reference line gives an indication of the tolerance of this type of driven qubit to uncertainties in the qubit frequency, which in this case is approximately 230 kHz.

In Fig. 3d, the microwave is amplitude-modulated with a sinusoid according to ref. 7, using the same average microwave power as in Fig. 3c. The period of the sinusoidal modulation is set to the theoretical optimal $T_{mod} = 1.8\,\mu s$, which is determined by the Rabi frequency obtained at this set power[6] ($T_{mod}\Omega_R = 1.8$) (see Supplementary Note 2). Comparing the range between the dashed lines in this modulated case (approximately 1.27 MHz) we can see a fivefold improvement in tolerance for the qubit detuning. This is further emphasised in the fitted Rabi coherence times plotted in Fig. 3e and f.

The sinusoidal modulation improves the tolerance of the architecture to the variability in Larmor frequencies for large arrays of spin qubits and also offers protection against microwave amplitude errors. If an ensemble of qubits have slightly different Rabi frequencies, a constant power microwave drive will cause the qubits to drift apart over time, whereas a sinusoidal modulation will cancel out the differences in rotation speed and always bring the qubits back to the initial state. This was predicted from theory in ref. 7.

Addressability of quasi-degenerate spins

Individual control of driven qubits is achieved by dynamically shifting the qubit frequency leveraging the Stark effect created by the voltage bias at the top gate that forms the dot[6–8]. In the case of two neighbouring qubits, the small separation between dots leads to crosstalk effects, whereby the frequency of a qubit is affected by the top gate of the neighbouring dot as well[40]. In the general case, this leads to the requirement for simultaneous pulsing on both gates to address one of the qubits without affecting the other.

SiMOS spin qubits are known to exhibit weak spin-orbit coupling, which is further minimised by pointing the static magnetic field along {100}[14]. While this is advantageous to achieve degeneracy between the spins, it also impacts the magnitude of the Stark shifts from the top gates[3,14]. Fortunately, only a small shift (<10% of Ω_R) is required for qubit control. In fact, too large shifts would cause the rotating wave approximating (RWA) to break[41], and moreover, would leave the qubits more susceptible to electrical noise. In this device, we are able to Stark shift Q2 by ~200 kHz using gate P2 in Fig. 4a, compared to a Rabi frequency of 1 MHz.

We find that the effect of gate P2 on Q2 is ~4 times stronger than on Q1. This strong differential Stark shift control is sufficient to achieve good addressability of Q2. We note that the inverse was not true and we did not perform operations using P1. In the future the g-factor can potentially be tuned by the magnetic field angle[3], once larger microwave driving amplitudes can be applied and the magnetic field angle is not required as a knob to reduce Larmor frequency spread. This would allow for direct control of Q1 with P1. Instead, we perform all single qubit gates in the same dot using P2 only and perform SWAP operations to address both qubits. In Fig. 4c and d, individual control of both qubits is shown with positive y-rotation on Q1 and negative y-rotation on Q2 for different P2 voltage amplitudes and different initial states. The initial state is determined by a microwave pulse applied to the degenerate qubits in the $|\downarrow\uparrow\rangle$ state, similar to what was done in Fig. 2d–f. In Fig. 4e and f, the same sequence is used but with positive rotations on both qubits. Together, the data in Fig. 4c, d and e, f demonstrate universal single-qubit control.

The single-qubit gate duration is $6 \times T_{mod}$ and the SWAP duration $1 \times T_{mod}$ with $T_{mod} = 1.8\,\mu s$. T_{mod} can be reduced by increasing Ω_R proportionally. The total sequence duration of $> 23\,\mu s$ in Fig. 4 leads to a significantly reduced visibility similar to Fig. 3d.

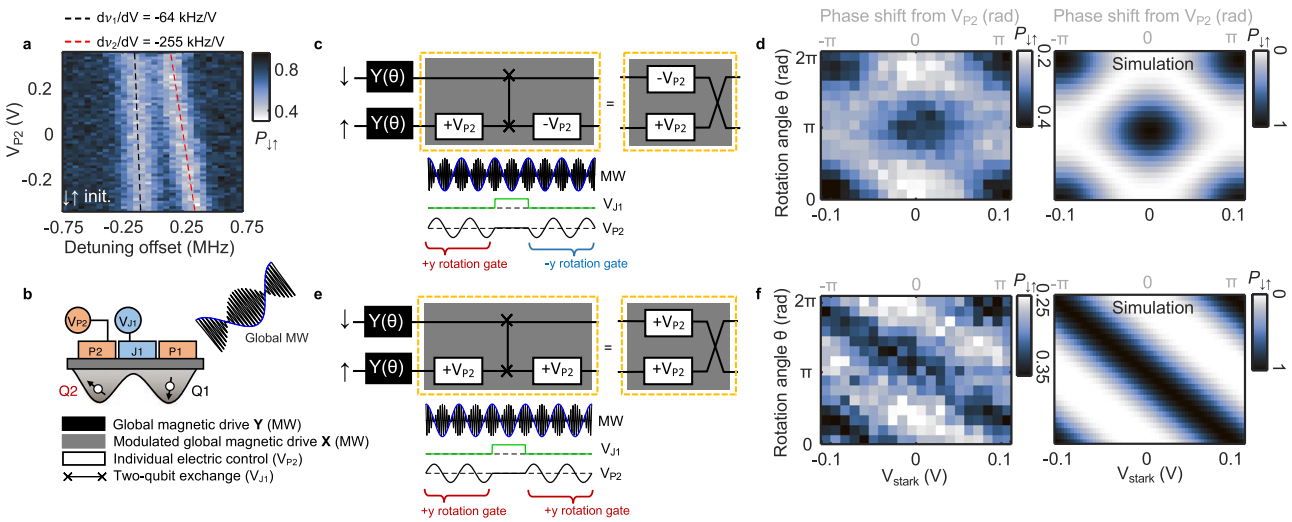

Fig. 4 | Addressability of quasi-degenerate spins. a Stark shifts of the Larmor frequencies ν_1 and ν_2 with the voltage on gate P2. **b** Schematic of double dot and the relevant control knobs P2, J1 and global microwave. **c** Gate sequence implementing single-qubit y-rotations of both qubits under gate P2 by using a SWAP gate. The gate on Q1 and Q2 have opposite signs. A simplified gate sequence is also shown. **d** Experimental results and simulations for the sequence in (**c**). **e**, **f** Identical sequence as in (**c**) and (**d**) but with equal sign on the single-qubit gates. The single-qubit gates last for six periods of the global field [two periods shown in schematic (**c**, **e**)] and the SWAP gate for one period.

Discussion

We have shown that two degenerate spins can be driven synchronously with a single global field and universally controlled electrically by local electrodes. This represents an alternative control strategy tackling the inevitable problem of frequency crowding in large arrays of spins. The spins are continuously decoupled from environmental noise by driving them on-resonance throughout any computation. We find that the driving is particularly important during entangling gates between spin states that are exposed to dephasing. In summary, this work represents a paradigm shift in qubit control strategies using dressed degenerate spins for noise-robust and scalable universal control. To overcome variability in Larmor and Rabi frequencies, smaller static magnetic field magnitudes and larger microwave driving amplitudes can be applied. Improved microwave engineering will also be important to produce a stronger and more uniform global magnetic field.

Methods

Experimental setup

The SiMOS quantum dot device is fabricated using 800 ppm isotopically purified ^{28}Si with a gate stack of Al/AlO_x oxide. It is the same device as device A in ref. 42 operated in isolated mode, that is, electrically isolated from the nearby electron reservoirs. The electron configuration is (3,3), except for Fig. 1f which is (1,3). The two dots are formed under gates P1 and P2. The gate J1 is used to control the exchange coupling between the spins. A global field is generated with an on-chip ESR antenna. Spin information is read out with a single-electron-transistor (SET) using Pauli spin blockade (PSB).

The experiments are done in an Oxford Kelvinox 400HA dilution refrigerator. DC bias voltages are coming from Stanford Research Systems SIM928 Isolated Voltage Sources. Gate pulse waveforms are generated with a Quantum Machines (QM) OPX+ and combined with DC biases using custom linear bias combiners at room temperature. The SET current is amplified using a room temperature I/V converter (Basel SP983c) and sampled by a QM OPX+. The microwave pulses are generated with a Keysight PSG8267D Vector Signal Generator, with I/Q and pulse modulation waveforms generated from the QM OPX+. The vector magnet is an Oxford instruments MercuryiPS.

The only feedback protocol used in this work is on the SET top gate, monitoring the current I_{SET} to maintain maximum sensitivity[43].

Interleaved measurements

The data displayed in Fig. 2a–c, d–f, g–i and c–d are all taken in an interleaved manner including two or three data sets. An interleaved measurement protocol involves acquiring a single data point for each data set before stepping the measurement parameters so that data points are acquired for each data set sequentially. This reduces temporal bias when trying to make a fair comparison between data sets.

Data availability

The data from this study have been deposited in a Zenodo repository (https://doi.org/10.5281/zenodo.13143835).

Code availability

The analysis codes that support the findings of the study are available from the corresponding authors on request.

References

1. Fowler, A. G., Mariantoni, M., Martinis, J. M. & Cleland, A. N. Surface codes: towards practical large-scale quantum computation. *Phys. Rev. A* **86**, 032324 (2012).
2. Franke, D. P., Clarke, J. S., Vandersypen, L. M. & Veldhorst, M. Rent's rule and extensibility in quantum computing. *Microprocessors Microsyst.* **67**, 1–7 (2019).
3. Cifuentes, J. D. et al. Bounds to electron spin qubit variability for scalable CMOS architectures. *Nat. Commun.* **15**, 4299 (2024).
4. Kane, B. E. A silicon-based nuclear spin quantum computer. *Nature* **393**, 133–137 (1998).
5. Seedhouse, A. E. et al. Quantum computation protocol for dressed spins in a global field. *Phys. Rev. B* **104**, 235411 (2021).
6. Hansen, I. et al. Implementation of an advanced dressing protocol for global qubit control in silicon. *Appl. Phys. Rev.* **9**, 031409 (2022).
7. Hansen, I. et al. Pulse engineering of a global field for robust and universal quantum computation. *Phys. Rev. A* **104**, 062415 (2021).
8. Laucht, A. et al. A dressed spin qubit in silicon. *Nat. Nanotechnol.* **12**, 61–66 (2017).
9. Vahapoglu, E. et al. Single-electron spin resonance in a nanoelectronic device using a global field. *Sci. Adv.* **7**, eabg9158 (2021).
10. Vahapoglu, E. et al. Coherent control of electron spin qubits in silicon using a global field. *npj Quantum Inf.* **8**, 126 (2022).
11. Veldhorst, M. et al. An addressable quantum dot qubit with fault-tolerant control-fidelity. *Nat. Nanotechnol.* **9**, 981–985 (2014).
12. Fogarty, M. et al. Integrated silicon qubit platform with single-spin addressability, exchange control and single-shot singlet-triplet readout. *Nat. Commun.* **9**, 4370 (2018).
13. Takeda, K. et al. A fault-tolerant addressable spin qubit in a natural silicon quantum dot. *Sci. Adv.* **2**, e1600694 (2016).
14. Tanttu, T. et al. Controlling spin-orbit interactions in silicon quantum dots using magnetic field direction. *Phys. Rev. X* **9**, 021028 (2019).
15. Harvey-Collard, P. et al. Spin-orbit interactions for singlet-triplet qubits in silicon. *Phys. Rev. Lett.* **122**, 217702 (2019).
16. Martinez, B. & Niquet, Y.-M. Variability of electron and hole spin qubits due to interface roughness and charge traps. *Phys. Rev. Appl.* **17**, 024022 (2022).
17. Tokura, Y., van der Wiel, W. G., Obata, T. & Tarucha, S. Coherent single electron spin control in a slanting zeeman field. *Phys. Rev. Lett.* **96**, 047202 (2006).
18. Philips, S. G. J. et al. Universal control of a six-qubit quantum processor in silicon. *Nature* **609**, 919–924 (2022).
19. Takeda, K. et al. Quantum tomography of an entangled three-qubit state in silicon. *Nat. Nanotechnol.* **16**, 965–969 (2021).
20. Pioro-Ladriere, M. et al. Electrically driven single-electron spin resonance in a slanting zeeman field. *Nat. Phys.* **4**, 776–779 (2008).
21. Lawrie, W. I. L. et al. Simultaneous single-qubit driving of semiconductor spin qubits at the fault-tolerant threshold. *Nat. Commun.* **14**, 3617 (2023).
22. Hendrickx, N. W. et al. A four-qubit germanium quantum processor. *Nature* **591**, 580–585 (2021).
23. Lawrie, W. I. L. et al. Spin relaxation benchmarks and individual qubit addressability for holes in quantum dots. *Nano Lett.* **20**, 7237–7242 (2020).
24. Jones, C. et al. Logical qubit in a linear array of semiconductor quantum dots. *Phys. Rev. X* **8**, 021058 (2018).
25. Meunier, T., Calado, V. E. & Vandersypen, L. M. K. Efficient controlled-phase gate for single-spin qubits in quantum dots. *Phys. Rev. B* **83**, 121403 (2011).
26. Vallabhapurapu, H. H. et al. High-fidelity control of a nitrogen-vacancy-center spin qubit at room temperature using the sinusoidally modulated, always rotating, and tailored protocol. *Phys. Rev. A* **108**, 022606 (2023).
27. Ferdous, R. et al. Interface-induced spin-orbit interaction in silicon quantum dots and prospects for scalability. *Phys. Rev. B* **97**, 241401 (2018).
28. Laucht, A. et al. High-fidelity adiabatic inversion of a 31P electron spin qubit in natural silicon. *Appl. Phys. Lett.* **104**, 092115 (2014).
29. Seedhouse, A. E. et al. Pauli blockade in silicon quantum dots with spin-orbit control. *PRX Quantum* **2**, 010303 (2021).

30. Gilbert, W. et al. On-demand electrical control of spin qubits. *Nat. Nanotechnol.* **18**, 131–136 (2023).
31. Loss, D. & DiVincenzo, D. P. Quantum computation with quantum dots. *Phys. Rev. A* **57**, 120–126 (1998).
32. Petta, J. R. et al. Coherent manipulation of coupled electron spins in semiconductor quantum dots. *Science* **309**, 2180–2184 (2005).
33. He, Y. et al. A two-qubit gate between phosphorus donor electrons in silicon. *Nature* **571**, 371–375 (2019).
34. Petit, L. et al. Design and integration of single-qubit rotations and two-qubit gates in silicon above one kelvin. *Commun. Mater.* **3**, 82 (2022).
35. Sigillito, A. J., Gullans, M. J., Edge, L. F., Borselli, M. & Petta, J. R. Coherent transfer of quantum information in a silicon double quantum dot using resonant SWAP gates. *npj Quantum Inf.* **5**, 110 (2019).
36. Watson, T. F. et al. A programmable two-qubit quantum processor in silicon. *Nature* **555**, 633–637 (2018).
37. Xue, X. et al. Quantum logic with spin qubits crossing the surface code threshold. *Nature* **601**, 343–347 (2022).
38. Huang, J. Y. et al. High-fidelity operation and algorithmic initialisation of spin qubits above one kelvin. *Nature* **627**, 772–777 (2024).
39. Ni, M. et al. A SWAP gate for spin qubits in silicon. *Preprint at arXiv* https://arxiv.org/pdf/2310.06700.pdf (2023).
40. Cifuentes, J. D. et al. Impact of electrostatic crosstalk on the spin qubits of dense CMOS architectures. *Preprint at arXiv*https://arxiv.org/pdf/2309.01849.pdf (2023).
41. Laucht, A. et al. Breaking the rotating wave approximation for a strongly driven dressed single-electron spin. *Phys. Rev. B* **94**, 161302 (2016).
42. Tanttu, T., Lim, W. H., Huang, J. Y. et al. Assessment of the errors of high-fidelity two-qubit gates in silicon quantum dots. *Nat. Phys.* (2024). https://doi.org/10.1038/s41567-024-02614-w.
43. Yang, C. H., Lim, W. H., Zwanenburg, F. A. & Dzurak, A. S. Dynamically controlled charge sensing of a few-electron silicon quantum dot. *AIP Adv.* **1**, 042111 (2011).

Acknowledgements

We acknowledge support from the Australian Research Council (FL190100167 and CE170100012), the U.S. Army Research Office (W911NF-23-10092) and the NSW Node of the Australian National Fabrication Facility. The views and conclusions contained in this document are those of the authors and should not be interpreted as representing the official policies, either expressed or implied, of the Army Research Office or the U.S. Government. The U.S. Government is authorised to reproduce and distribute reprints for Government purposes notwithstanding any copyright notation herein. I.H., A.E.S., S.S., M.K.F., J.Y.H., and A.N. acknowledge support from Sydney Quantum Academy.

Author contributions

C.H.Y., A.S.D., I.H., A.S. and A.L. conceived the project and experiments. A.E.S. and M.K.F. developed theoretical models. W.H.L. and F.E.H. fabricated the device. K.M.I. prepared and supplied the ^{28}Si epilayer wafer. S.S., J.Y.H., N.D.S. and T.T. assisted in experiments and with the cryogenic measurement setup. I.H. and A.N. performed the experiments. I.H. and C.H.Y. analysed the data and wrote the manuscript with input from all the authors.

Competing interests

A.S.D. is CEO and a director of Diraq Pty Ltd. T.T., N.D.S., W.H.L., F.E.H., A.S., A.L., A.S.D., and C.H.Y. declare equity interest in Diraq Pty Ltd. I.H., A.E.S., A.S., C.H.Y., A.L., and A.S.D. are inventors on a patent related to this work (PCT 2023004469) filed by the University of New South Wales. The remaining authors declare no competing interests.

Additional information

Supplementary information The online version contains supplementary material available at https://doi.org/10.1038/s41467-024-52010-4.

Correspondence and requests for materials should be addressed to Ingvild Hansen, Andrew S. Dzurak or Chih Hwan Yang.

Peer review information *Nature Communications* thanks Andrew Ramsay, and the other, anonymous, reviewer for their contribution to the peer review of this work. A peer review file is available.